Near-Optimal Moiré Grating for Chaotic Dynamic Visual Cryptography

Rita Palivonaite[1], Algimantas Fedaravicius[2], Algiment Aleksa[1], and Minvydas Ragulskis[1]

[1] Research Group for Mathematical and Numerical Analaysis of Dynamical Systems Kaunas University of Technology, Studentu 50-222, Kaunas LT-51368, Lithuania
[2] Institute of Defence Technologies, Kaunas University of Technology, Kestucio 27, LT-44312, Lithuania

Abstract. Image hiding based on chaotic oscillations and near-optimal moiré gratings is presented in this paper. The secret image is embedded into a single cover image. The encrypted secret image appears in a form of time-averaged moiré fringes when the cover image is oscillated in a predefined direction, according to a chaotic law of motion. The criterion of the optimality of a moiré grating is based on the absolute difference between the standard deviation of time-averaged images of near-optimal moiré gratings in the background and in the zones associated to the secret image. Genetic algorithms are used for the identification of a near-optimal set of moiré gratings for image hiding applications. Numerical experiments are used to illustrate the functionality of the method.

Keywords: Visual cryptography, Time-averaged moiré fringes, Chaotic oscillations.

1 Introduction

Visual cryptography is a cryptographic technique which allows visual information (pictures, text, etc.) to be encrypted in such a way that the decryption becomes a mechanical operation that does not require a computer. Visual cryptography was pioneered by Naor and Shamir (1994) [1]. They presented a visual secret sharing scheme, where an image is divided into n shares. Only one who has all n shares could reveal the secret image. Each share is printed on a separate transparency, and visual decryption is performed by overlaying all n shares.

Since 1994, many advances in visual cryptography have been done. Visual cryptography scheme for grey level images is proposed in [2], a necessary and sufficient conditions are given for such scheme to exist. Three methods for visual cryptography for gray level and color images is introduced in [3]. Efficient visual secret sharing scheme for color images by using pixel expansion is proposed by [4]. Probabilistic k out of n visual cryptographic schemes for grayscale and color images are presented in [5]. Visual secret sharing schemes for multiple images are demonstrated in [6–8]. Multi-secret image sharing scheme based on Boolean operations is introduced in [9] where the proposed method not only keeps the

secret images confidential but also increases the capacity of sharing multiple secrets. Algorithms of encryption based on random grids and multiple random grids are adopted for grayscale level and color images by [10, 11]. Multiple secret images are encrypted by circular random grids and presented by [12]. All these visual secret sharing schemes are based on the fact that the secret image is encrypted into two or more images (shares). The computer is used to embed the secret image into the background moiré grating but the decryption of the secret image is completely visual and does not require the computer equipment [13, 14].

Single share technique is introduced in [15, 16]. This kind of encryption is based on time-averaging moiré methods. The encrypted cover image has to be oscillated in order to produce time averaged moiré fringes. These fringes are visualized when the encoded image is oscillated in a predefined direction, at a proper amplitude of harmonic oscillations. Moreover, different moiré gratings can be used for the encryption of the secret image. Harmonic moiré grating and harmonic oscillations are used in [15]. Stepped moiré grating and triangular waveforms are used in [16].

It is important to note that the selection of the moiré grating and type of oscillation must be pre-chosen before the secret image is encrypted into the cover image. Not every moiré grating produces time-averaged fringes. It is shown by [15] that the stepped moiré grating does not produce time-averaged moiré fringes when the encoded image is harmonically oscillate even at appropriate amplitude and direction of oscillations. Image hiding technique based on time-average fringes produced by rectangular waveforms and near-optimal moiré gratings is presented in [17]. Evolutionary algorithms are used here to find near optimal moiré grating.

The ability to embed a secret image into a single cover image opens a possibility to exploit dynamic visual cryptography in vibration control applications [18]. But so far, only harmonic and rectangular waveforms had been considered for dynamic visual cryptography. It is clear that different type of complex nonlinear structures would perform chaotic vibrations even under harmonic loads. Thus, the main objective of this presentation is to develop a framework for chaotic dynamic visual cryptography. Moreover, it is completely unclear what types of moiré gratings would be advantageous for chaotic oscillations. Therefore, the second objective of this paper is to identify a near optimal moiré grating and to demonstrate its applicability for chaotic visual cryptography.

2 Optical Background

One-dimensional moiré grating is considered in this paper. First of all we define requirements for the grayscale function $F(x)$:

(i) Function $F(x)$ is a periodic function $F(x+\lambda) = F(x)$, where λ is the pitch of grating.

(ii) All values of the grayscale function $F(x)$ belongs to a closed interval $F(x) \in [0;1]$, where 0 corresponds to the black color; 1 – to white color; all inter-

mediate numerical values of the grating correspond to an appropriate grayscale level.

(iii) $F(x)$ is an integrable function – it has only a finite number of discontinuity points in every finite interval [0;1]

(iv) The range of grayscale grating values spans through the whole grayscale interval.

We will use an m-pixels grayscale grating function $F_{m,n}(x)$ in this paper. It is defined as follows:

$$F_{m,n}(x) = y_k \tag{1}$$

where x belongs to a closed interval $\left[\frac{(k-1)\lambda}{m} + j\lambda;\ \frac{k\lambda}{m} + j\lambda\right]$; $k = 1,2\ldots,m$; $j \in Z$ and y_k, $k = 1,2\ldots,m$ are grayscale levels. Thus the size of a single pixel is $\frac{\lambda}{m}$; m pixels fit into one period of the grayscale function.

For example, $F_{22,32}(x)$ represents a grayscale grating function which period is composed from 22 pixels and the grayscale level of every pixel can be selected from 32 different levels (all levels are in-between 0 and 1). Function $F_{22,32}(x)$ can be expanded into the Fourier series:

$$F(x) = \frac{a_0}{2} + \sum_{k=1}^{\infty}\left(a_k \cos\frac{2\pi kx}{\lambda} + b_k \sin\frac{2\pi kx}{\lambda}\right) \tag{2}$$

where a_k,$b_k \in R$; $k = 1,2,\ldots$. Parameters of the Fourier expansion of $F(x)$ read:

$a_0 = \frac{2}{m}\sum_{k=1}^{m} y_k$; $a_k = \frac{1}{k\lambda}\sum_{j=2}^{m}\left((y_{j-1} - y_j)\sin\frac{2(j-1)k\pi}{m}\right)$; and

$b_k = -\frac{1}{k\lambda}\sum_{j=2}^{m}\left((y_{j-1} - y_j)\cos\frac{2(j-1)k\pi}{m}\right)$; $k = 1,2,\ldots$.

Let us consider a situation when the described one-dimensional moiré grating is oscillated in the direction of the x-axis and time-averaging optical techniques are used to register the time-averaged image. Time-averaging operator H_s describing the grayscale level of the time-averaged image is defined as [19]:

$$H_s(x \mid F;\xi_s) = \lim_{T\to\infty}\frac{1}{T}\int_0^T F(x - \xi_s(t))\,dt \tag{3}$$

where t is time; T is the exposure time; $\xi_s(t)$ is a function describing dynamic deflection from the state of equilibrium; $s \geq 0$ is a real parameter; $x \in R$. It is shown in [16] that if the density function $p_s(x)$ of the time function $\xi_s(t)$ is symmetric, then the time-averaged image of the moiré grating oscillated according to the time function reads:

$$H_s(x \mid F;\xi_s) = \frac{a_0}{2} + \sum_{k=1}^{\infty}\left(\left(a_k \cos\frac{2\pi kx}{\lambda} + b_k \sin\frac{2\pi kx}{\lambda}\right)\right) P_s\left(\frac{2\pi ks}{\lambda}\right) \tag{4}$$

where the notation P_s is used for the Fourier transform of the density function $p_s(x)$. In other words, the time-averaged image is the convolution of the

static image (the cover image) and the point-spread function determining the oscillation of the original image [20, 21].

Let us require that $\xi_\sigma(t)$ is a Gaussian normal ergodic process with zero mean and σ^2 variance. The standard deviation σ is used in the subscript instead of the parameter s in Eq. (3). Then, the density function $p_\sigma(x)$ reads:

$$p_\sigma(x) = \frac{1}{\sqrt{2\pi}\sigma} \exp\left(-\frac{x^2}{2\sigma^2}\right) \tag{5}$$

and the Fourier transform of $p_\sigma(x)$ takes the form:

$$p_\sigma(\omega) = \exp\left(-\frac{1}{2}(\omega\sigma)^2\right) \tag{6}$$

Then, the time-averaged image of the moiré grating oscillated by a Gaussian time function reads [22]:

$$H_s(x \mid F;\xi_\sigma) = \frac{1}{2} + \sum_{k=1}^{+\infty}\left(a_k \cos\left(\frac{2\pi k x}{\lambda}\right) + b_k \sin\left(\frac{2\pi k x}{\lambda}\right)\right) \cdot \exp\left(-\frac{1}{2}\left(\frac{2\pi k\sigma}{\lambda}\right)^2\right) \tag{7}$$

Equation 7 describes the formation of the time-averaged image as the exposure time tends to infinity and the oscillation of original moiré grating is governed by the function $\xi_\sigma(t)$.

The mean of a time-averaged grayscale function is defined as [17]:

$$E(H_s(x \mid F;\xi_s)) = \frac{1}{\lambda}\int_0^\lambda H_s(x \mid F;\xi_s)\,dx = \frac{a_0}{2} \tag{8}$$

Finally, the standard of a time-averaged grayscale grating function reads:

$$\sigma(H_s(x \mid F;\xi_s)) = \sqrt{\frac{1}{\lambda}\int_0^\lambda \left(H_s(x \mid F;\xi_s) - E(H_s(x \mid F;\xi_s))\right)^2 dx} \tag{9}$$

In this paper we consider the oscillation of a grayscale grating function $F_{m,n}(x)$ according to the Gaussian time function. Therefore, the standard of such time-averaged image reads:

$$s = \sigma(H_s(x \mid F;\xi_s)) = \frac{\sqrt{2}}{2}\sqrt{\sum_{k=1}^{\infty}(a_k^2 + b_k^2)\exp\left(-\left(\frac{2\pi k\sigma}{\lambda}\right)^2\right)} \tag{10}$$

3 Perfect Grayscale Functions and their Fitness Assessment

3.1 The Definition of a Perfect Grayscale Function

As mentioned previously, we will use an m-pixels grayscale grating function $F_{m,n}(x)$. It is clear that unrestricted random selection of grayscale pixels' levels may result is such moiré gratings which would be hardly applicable for image hiding applications. Therefore we introduce four additional requirements. Grayscale functions satisfying these requirements will be entitled as perfect grayscale functions.

Requirement 1. Grayscale levels of pixels in the grating span over the whole grayscale interval [0;1].

Requirement 2. The average grayscale level in a period is equal to 0.5.

Requirement 3. The norm of the grayscale grating function must be greater than or equal to the half of the norm of the harmonic grayscale function: $\|F_{m,n}(x)\| \geq \left\|\frac{1}{2} + \frac{1}{2}\cos\left(\frac{2\pi}{\lambda}x\right)\right\| = \frac{1}{2\pi}$, where λ is the pitch of the harmonic grating; the norm is defined as follows [17]: $\|F(x)\| = \frac{1}{\lambda}\int_0^{\lambda}\left(F(x) - \frac{1}{2}\right)dx$.

Requirement 4. The main peak of the discrete Fourier amplitude spectrum at $\frac{2\pi}{\lambda}$ must be at least two times higher than all other peaks: $c_1 \geq 2c_k$, for all $k = 2,3,4,\ldots$, where $c_k = \sqrt{a_k^2 + b_k^2}$.

All four requirements are directly related to peculiarities of the visual decryption procedure based on the formation of time averaged moiré fringes. Requirement 1 requires using the whole range of grayscale levels in one pitch of the moiré grating. Requirement 2 demands that the grayscale level of a time-averaged moiré fringe is equal to 0.5. Requirement 3 forbids grayscale functions with small variation around 0.5. Requirement 4 forces that the pitch of a grating be clearly visible by a naked eye.

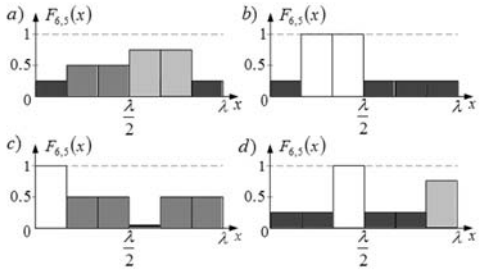

Fig. 1. Illustrations of non-perfect grayscale functions $F_{6,5}(x)$: a) - the whole grayscale range is not used (Requirement 1 does not hold); b) - the average grayscale level in a pitch does not equal to 0.5 (Requirement 2 does not hold); c) - the norm of the grayscale functions is too small (Requirement 3 does not hold); d) - the secondary harmonic is too high (Requirement 4 does not hold).

It is obvious that not all grayscale functions fulfil these four requirements. Let us perform a simple computational experiment. We will find the number of perfect grayscale functions of $F_{6,5}(x)$ (6 pixels in a period; each pixel can acquire 5 discrete grayscale levels). Computational costs of full sorting algorithm are not high; the number of all possible $F_{6,5}(x)$ functions is $5^6 = 15625$ (permutations with repetition). The percentage of $F_{6,5}(x)$ functions which meet according requirements are presented in Fig. 2. It can be noted that only about 1.728% of all grayscale grating functions $F_{6,5}(x)$ are perfect grayscale functions. We will use 22 pixels in the pitch of the grating and assume only 32 different discrete grayscale levels (instead of 256). Now, checking if a current $F_{6,5}(x)$ grayscale function is a perfect is a straightforward task (in opposite to the generation of the best perfect functions).

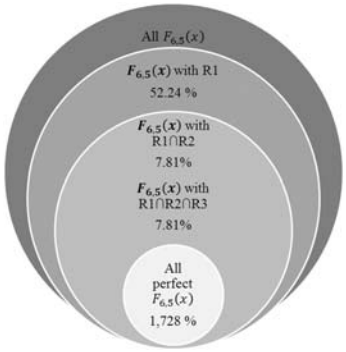

Fig. 2. Illustration of the percentage of $F_{6,5}(x)$ functions which meet the requirements (R1 stands for Requirement 1, R2 stands for Requirement 2, R3 stands for Requirement 3).

3.2 The Definition of the Fitness Value for a Grayscale Function

The next step is the definition of the fitness function for every grayscale function $F_{22,32}(x)$. We did use a 22 pixels in a pitch stepped moiré grating ($F_{22,2}(x)$) for the background and 20 pixels in a pitch stepped moiré grating ($F_{20,2}(x)$) for the secret image in [17]. We will use the same principle now – except that grayscale functions will be $F_{22,32}(x)$ and $F_{20,32}(x)$. In fact, we need to define the fitness function only for $F_{22,32}(x)$ - the function $F_{20,32}(x)$ can be produced from $F_{22,32}(x)$ by deleting two pixels which grayscale levels are closest to 0.5.

It is well known that chaotic oscillations do not produce time-averaged moiré fringes [16]. Anyway, the proposed visual cryptography scheme should be based on the differences between time-averaged images of $F_{22,32}(x)$ and $F_{20,32}(x)$ (even though time-averaged fringes would not form). The human eye does interpret a time-averaged moiré fringe if its standard (Eq. 6) is less than 0.03 [18]. We fix this value for chaotic oscillations also and mark it as δ in Fig. 3.

First of all we compute the decay of the standard s of the time-averaged image formed by $F_{22,32}(x)$ at increasing standard σ of the Gaussian time function (Eq. 10). Note that Fourier expansions coefficients a_k, b_k for a concrete realization of $F_{22,32}(x)$ must be computed in advance.

This decay of the standard s is illustrated by a thick solid line in Fig. 3. Next we truncate $F_{22,32}(x)$ to $F_{20,32}(x)$ and compute the decay of s again (coefficients a_k, b_k must be recalculated again); it is illustrated by a thick dotted line in Figure 3.

As soon as one of the two lines intersect the level δ, we fix the optimal value of σ for the best visual reconstruction of the encoded image. Moreover, we compute the difference between standards of time-averaged-images produced by $F_{22,32}(x)$ to $F_{20,32}(x)$ (shown by a thin solid vertical line in Figure 3). This difference between standards is denoted as $\varphi(F_{22,32}(x))$ and is denoted as the fitness of a grayscale function. Note that the fitness value can be computed for any grayscale function (not necessarily the perfect function). Also, we do not know which line (the solid or the dashed line) will intersect the δ-level first; the most important is just the absolute value of the difference between the standards ($\varphi(F_{22,32}(x)) \geq 0$). The higher is the fitness value, the better is the visual difference between the time averaged image of the background and the secret.

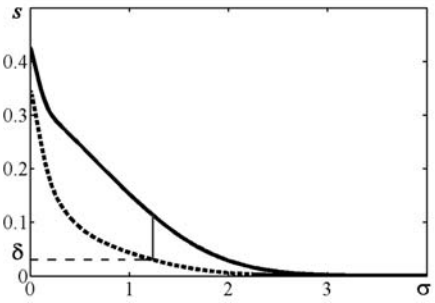

Fig. 3. Computation of the fitness value for $F_{22,32}(x)$. Decay of the standards of the time-averaged images of $F_{22,32}(x)$ and $F_{22,32}(x)$ are illustrated in the thick solid line and the dashed solid line accordingly. The fitness value $\varphi(F_{22,32}(x))$ is shown in thin vertical solid line.

Now, the selection of the best perfect grayscale function is fully defined. Unfortunately, a brute force full sorting algorithm is simply impossible due to the limited computational resources. Naturally, the alternative task is to seek near-optimal moiré gratings and use evolutionary algorithms for that purpose.

4 The Structure of the Genetic Algorithm

We construct the genetic algorithm for the identification of a near-optimal perfect grayscale function in such a way that every chromosome represents one period of the function $F_{22,32}(x)$. The length of each chromosome is 22; every gene is an integer number between 0 and 31 and represents a grayscale level for the respective pixel. Since we operate with perfect moiré gratings only, the modified fitness function $\Phi(F_{22,32}(x))$ takes the following form:

$$\Phi(F_{22,32}) = \begin{cases} 0 & \text{if } F_{22,32}(x) \text{ is not perfect} \\ \varphi(F_{22,32}) & \text{if } F_{22,32}(x) \text{ is perfect} \end{cases} \tag{11}$$

The initial population is composed of n randomly generated chromosomes with values of genes uniformly distributed over the interval [0;31]. The fitness of each perfect chromosome is evaluated and an even number of chromosomes is selected to the mating population. A random roulette method for the selection of chromosomes is used. The chance that the chromosome will be selected to the mating population is proportional to its fitness value. All chromosomes are paired when process of mating is over. The crossover between two chromosomes is executed for all pairs in the mating population. We use one-point crossover method and the location of this point is random. The crossover coefficient κ characterizes a probability that the crossover procedure will be executed for a pair of chromosomes.

In order to avoid convergence to one local solution we use a mutation procedure. The mutation parameter μ $(0 < \mu < 1)$ determines the probability for a chromosome to mutate. The quantity of chromosomes which are exposed to the mutation procedure is calculated as $n_m = round(\mu \cdot n)$. Then n_m chromosomes are selected randomly and one gene of each chromosome is changed by a random number $mod_{32}(\tau + r)$; here τ is the gene value before the modification; r is a random integer uniformly distributed over the interval [0;31].

In general, the selection of parameters of evolutionary algorithms is an empirical process, though some common principles are described in [23, 24]. The following parameters of the evolutionary algorithm must be pre-selected: the crossover coefficient κ; the mutation parameter μ; the size of the population n and the number of generations. We will use recommendations for parameters as it was pre-selected for near optimal perfect grayscale gratings in [17]. As it is recommended we fix values of parameters of the evolutionary algorithm ($\kappa = 0.7$ and incremental increase of μ from 0.05 till 0.5), the size of the population is $n = 20000$ and the number of generations is 10. The evolutionary algorithm is executed 5 times; the best generated perfect grating is selected then.

The best result of finding near-optimal perfect grayscale grating function $F_{22,32}(x)$ is presented in Fig. 4 part (a). We will use this perfect grayscale function for image hiding based on chaotic visual cryptography.

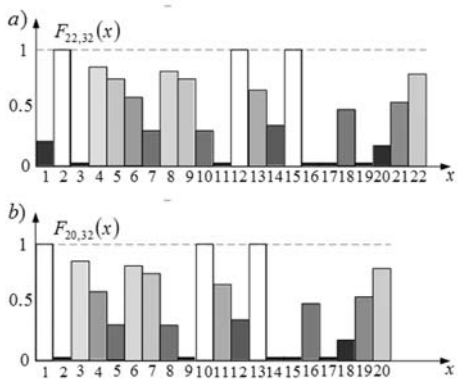

Fig. 4. Near-optimal perfect grayscale functions: a) $F_{22,32}(x)$ and b) $F_{20,32}(x)$.

5 Near-Optimal Chaotic Visual Cryptography

5.1 The Structure of the Cover Image

As mentioned previously As mentioned previously, the main objective of this paper is to find a near-optimal perfect moiré grating which can be adapted for image hiding based on time-averaged moiré fringes produced by chaotic oscillations.

The structure of the encoded cover image is analogous to the one used in [15]. We have to select two moiré gratings: the first for the secret image and the second for the background of the secret image. The pitch of the moiré grating of the secret image is $\lambda_0 = 22 \cdot 0.27\text{mm} = 5.94$ mm and the pitch of the moiré grating used for the background is $\lambda_1 = 20 \cdot 0.27\text{mm} = 5.40$ mm (the size of a pixel is assumed to be 0.27 mm for the monitor HP ZRW24; two different values 22 and 20 indicate the size of the pitches of moiré gratings used for the secret image and for the background).

As mentioned previously, the encoding process is similar to the one presented in [15]. Stochastic phase deflection and phase regularization algorithms are used to embed the secret into the cover image.

5.2 Computational Experiments

The dichotomous image in Fig. 5 will be used as a secret image in computational experiments with chaotic visual cryptography. The encoded cover image is shown in Figure 6. A human eye cannot distinguish the secret from the background.

The secret image cannot be visualized using harmonic oscillations at any amplitude. But it can be revealed using chaotic oscillations at $\sigma = 2.2$. The pure grey moiré fringes do not appear in a time-averaged image, but the difference between the background and the secret image is clearly visible (Fig. 7). Of course,

Fig. 5. The dichotomous secret image.

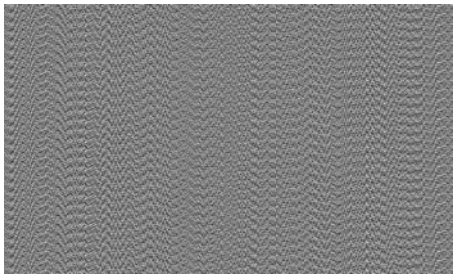

Fig. 6. The encoded cover image.

the secret image is not leaked if σ is substantially different from 2.2, nor for other non-chaotic waveforms.

Though the boundaries between the secret image and the background are clearly visible in Figure 7, it would be advantageous to use contrast enhancement techniques for highlighting the leaked image [18]; the highlighted secret image is shown in Figure 8.

6 Conclusions

A computational proof for the applicability of dynamic visual cryptography for chaotic oscillations is presented in this paper. The proposed technique can be applied for optical control of chaotic oscillations. Experimental (real-world) implementation of such an optical control method is a definite object of future research.

Acknowledgments. This research was funded by a grant (No. MIP-100/2012) from the Research Council of Lithuania.

Fig. 7. Computational decryption of the secret image when the encoded image is oscillated chaotically by the Gaussian law at $\sigma = 2.2$.

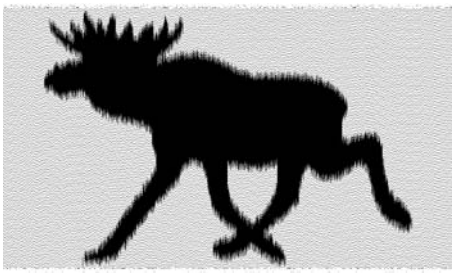

Fig. 8. Contrast enhancement of the decoded image.

References

1. Naor, M., and Shamir, A.: Visual cryptography, in "Advances in Cryptology - EUROCRYPT '94" Lecture Notes in Computer Science, 950 pp. 1–12. Springer-Verlag, Berlin (1995)
2. Blundo, C., De Santis A., Naor M..: Visual cryptography for grey level images. Inf. Process. Lett. 75, 6, 255–259 (2000)
3. Hou, Y.C.: Visual cryptography for color images. Pattern Recognition 36, 7, 1619–1629 (2003)
4. Shyu, S.J.: Efficient visual secret sharing scheme for color images. Pattern Recognition 39, 5, 866–880 (2006)
5. Wang, D., Yi, F., Li, X.: Probabilistic visual secret sharing schemes for grey-scale images and color images. Information Sciences 181, 11, 2189–2208 (2011)
6. Feng, J.B, Wu, H.C., Tsai, C.S., Chang, Y.F., Chu, Y.P.: Visual secret sharing for multiple secrets. Pattern Recognition 41, 12, 3572–3581 (2008)
7. Shyu, S.J., Huang, S.Y., Lee, Y.K., Wang, R.Z, Chen, K.: Sharing multiple secrets in visual cryptography. Pattern Recognition 40, 12, 3633–3651 (2007)
8. Lee, K.H., and Chiu, P.L.: A high contrast and capacity efficient visual cryptography scheme for the encryption of multiple secret images. Optics Communications 284, 12, 2730–2741 (2011)
9. Chen, T.H., Wu C.S.: Efficient multi-secret image sharing based on Boolean operations. Signal Processing 91, 1, 90–97 (2011)
10. Shyu, S.J.: Image encryption by random grids. Pattern Recognition 40, 3, 1014–1031 (2007)

11. Shyu, S.J.: Image encryption by multiple random grids. Pattern Recognition 42, 7, 1582–1596 (2009)
12. Chen, T.H., Li K.C.: Multi-image encryption by circular random grids. Information Sciences 189, 255–265 (2012)
13. Wang, R.Z., Lan Y.C., Lee, Y.K., Huang, S.Y, Shyu, S.J., Chia, T.L.: Incrementing visual cryptography using random grids. Optics Communications 283, 21, 4242–4249 (2010)
14. Chen, Y.C., Tsai, D.S., Horng, G.: A new authentication based cheating prevention scheme in Naor–Shamir's visual cryptography. Journal of Visual Communication and Image Representation 23, 8, 1225-33 (2012)
15. Ragulskis, M., Aleksa, A.: Image hiding based on time-averaging moiré. Optics Communications 282, 14, 2752–2759 (2009)
16. Ragulskis, M., Aleksa, A., Navickas, Z.: Image hiding based on time-averaged fringes produced by non-harmonic oscillations. Journal of Optics A: Pure and Applied Optics 11, 12, 125411 (2009)
17. Sakyte, E., Palivonaite, R., Aleksa, A., Ragulskis, M.: Image hiding based on near-optimal moiré gratings. Optics Communications 284, 16-17, 3954–3964 (2011)
18. Petrauskiene, V., Aleksa A., Fedaravicius A., Ragulskis M.: Dynamic visual cryptography for optical control of vibration generation equipment. Optics and Lasers in Engineering 50, 6, 869–876 (2012)
19. Ragulskis, M., Navickas, Z.: Hash function construction based on time averaged moiré. Discrete and Continuous Dynamical Systems - Series B 8, 4, 1007–1020 (2007)
20. Fujji, H., Asakura, T.: Effect of the point spread function on the average contrast of image speckle patterns. Optics Communications 21, 80–84 (1977)
21. Braat, J.J.M., van Haver S., Janssen A.J.E.M., Dirksen, P.: Assessment of optical systems by means of point-spread functions. Progress in Optics 51, 6, 349–468 (2008)
22. Ragulskis, M., Sanjuan, M.A., Saunoriene L.: Applicability of time-average moiré techniques for chaotic oscillations. Physical Review E 79, 3, 036208 (2007)
23. Holland, J.H.: Adaptation in Natural and Artificial Systems: An Introductory Analysis with Application to Biology, Control, and Artificial Intelligence. 2nd ed. The MIT Press, Cambridge (1992)
24. Whitley, D.: A genetic algorithm tutorial. Statistics Computing 4, 2, 65–85 (1994)